The FASEB Journal article fj.201700064R. Published online April 18, 2017.

THE FASEB JOURNAL • RESEARCH • www.fasebj.org

Adeno-associated viral 9–mediated Cdk5 inhibitory peptide reverses pathologic changes and behavioral deficits in the Alzheimer's disease mouse model

Yong He,[*,†] Suyue Pan,[*] Miaojing Xu,[*] Rongni He,[‡] Wei Huang,[‡] Pingping Song,[*] Jianou Huang,[§] Han-Ting Zhang,[¶,‖] and Yafang Hu[*,1]

[*]Department of Neurology, Nanfang Hospital, Southern Medical University, Guangzhou, China; [†]Department of Neurology, First People's Hospital of Chenzhou, Chenzhou, China; [‡]Department of Neurology, Zhujiang Hospital, Southern Medical University, Guangzhou, China; [§]Department of Neurology, 421 Hospital, Guangzhou, China; and [¶]Department of Behavioral Medicine and Psychiatry and [‖]Department of Physiology and Pharmacology, West Virginia University Health Sciences Center, Morgantown, West Virginia, USA

ABSTRACT: Cyclin-dependent kinase 5 (Cdk5), which binds to and is activated by p35, phosphorylates multiple substrates and plays an essential role in the development and function of the CNS; however, proteolytic production of p25 from p35 under stress conditions leads to the inappropriate activation of Cdk5 and contributes to hyperphosphorylation of τ and other substrates that are related to the pathogenesis of Alzheimer's disease. Selective inhibition of aberrant Cdk5 activity *via* genetic overexpression of Cdk5 inhibitory peptide (CIP) reduces pathologic changes and prevents brain atrophy and memory loss in p25-transgenic mice. In the present study, we delivered adeno-associated viral 9 carrying green fluorescent protein–CIP (AAV9-GFP-CIP) to brain cells *via* intracerebroventricular infusion in amyloid precursor protein/presenilin 1 (APP/PS1) double-transgenic 3-mo-old mice after the occurrence of β-amyloid (Aβ) aggregation and the hyperphosphorylation of τ. Three months of treatment of AAV9-GFP-CIP reduced pathologic changes, including τ hyperphosphorylation, (Aβ) deposit, astrocytosis, and microgliosis, which were correlated with the reversal of memory loss and anxiety-like behavior observed in APP/PS1 mice. The neuroprotection effect of AAV9-GFP-CIP lasted an additional 7 mo—the end point of the study. These findings provide a novel strategy to selectively target Cdk5 for the treatment of Alzheimer's disease.—He, Y., Pan, S., Xu, M., He, R., Huang, W., Song, P., Huang, J., Zhang, H.-T., Hu, Y. Adeno-associated viral 9–mediated Cdk5 inhibitory peptide reverses pathologic changes and behavioral deficits in the Alzheimer's disease mouse model. FASEB J. 31, 000–000 (2017). www.fasebj.org

KEY WORDS: AAV9 · CIP · tau pathology · β-amyloid

Alzheimer's disease (AD) is one of the leading and currently incurable neurodegenerative diseases in the aging population. There are 2 pathologic hallmarks of AD, including extracellular senile plaques formed by deposition of β-amyloid (Aβ) peptide and intracellular aggregations of neurofibrillary tangles (NFTs) that mainly contain hyperphosphorylated τ (1). Complex triggers, including inflammation and excitotoxic and oxidative stress, may contribute to Aβ burden and/or tauopathy (2–4).

Neuronal cells are enriched with p35, which binds to and activates cyclin-dependent kinase 5 (Cdk5). Cdk5/p35 activity is required for neurons fundamental functions (4–6); however, cleavage of p35 into p25 by calpain under stress conditions leads to neurotoxin (7). In postmortem brains of patients with AD, accumulation of p25 correlates with Cdk5/p25 hyperactivity in NFTs (7). Cdk5 induces τ hyperphosphorylation and the accumulation of NFTs in transgenic (Tg) mice that overexpress p25 (8, 9). Accumulated evidence from postmortems and animal models has demonstrated that deregulation of Cdk5 also contributes to the pathogenesis of several other degenerative diseases, including Parkinson's disease (10), amyotrophic lateral sclerosis (11, 12), and ischemia stroke (13), which suggests that Cdk5 may represent a promising therapeutic target for such neurodegenerative diseases as AD.

Accordingly, Cdk5 inhibitors, such as roscovitine, that target ATP binding sites of Cdk5 have been considered as potential therapeutic agents; however, these compounds could produce serious adverse effects as a result of the

ABBREVIATIONS: Aβ, β-amyloid; AAV, adeno-associated viral; AD, Alzheimer's disease; APP, amyloid precursor protein; Cdk5, cyclin-dependent kinase 5; CIP, Cdk5 inhibitory peptide; GFAP, glial fibrillary acidic protein; GFP, green fluorescent protein; HEK293T, human embryonic kidney 293T; i.c.v., intracerebroventricular; IHC, immunohistochemistry; NFT, neurofibrillary tangle; PS1, presenilin 1; SYN, synapsin; Tg, transgenic; vg, vector genome; WT, wild type

[1] Correspondence: Department of Neurology, Nanfang Hospital, Southern Medical University, 1838 Guangzhou Ave. North, Guangzhou, Guangzhou 510515, China. E-mail: yafanghu@smu.edu.cn

doi: 10.1096/fj.201700064R

nonselective inhibition of other Cdks (13–15). Several p35-derived peptides have been identified as another category of Cdk5-specific inhibitory peptides. CIP (Cdk5 inhibitory peptide; amino acid residue, aa 154–279 of p35) is the first identified peptide that displays a specific inhibitory effect on the activity of Cdk5/p25, but not Cdk5/p35, and prevents neuronal apoptosis *in vitro* (16, 17). Furthermore, in p25-inducible double-Tg mice, constitutive expression of CIP in the forebrain reduces p25-mediated neurodegeneration and improves cognitive performance in CIP-p25 tetra-Tg mice (18). CIP does not affect Cdk5/p35 function as CIP-Tg mice seemed to be phenotypically and developmentally normal; however, clinical translation of CIP is limited because of its difficulty in crossing the brain-blood barrier. The 24-aa peptide P5 truncated from CIP was later identified; it exhibits inhibitory activity similar to CIP *in vitro*. Modified P5 (TP5 or TFP5) with Tet peptide to facilitate brain-blood barrier penetration has been shown to exert neuron protection in 5×FAD mice, which carry 3 amyloid precursor protein (APP) mutations and 2 presenilin 1 (PS1) mutations (3). TP5 or TFP5 protect neurons from 1-methyl-4-phenyl-1,2,3,6-tetrahydropyridine insult in Parkinson's disease mouse models (19, 20).

Adeno-associated viral (AAV) vectors have been attractive delivery systems for gene therapy because they transduce nondividing cells with long-term, stable transgene expression and have a high degree of safety (21–25). CNS-directed AAV serotypes include AAV1, -2, -4, -5, -6, -8, -9, -10, and -11 (26). Specific knockdown of Cdk5 in the hippocampus by injection of microRNA-based short hairpin against CDK5 (shCDK5miR) prevents spatial memory dysfunction and τ pathology in 3×Tg AD mice, which harbor PS1(M146V), APP(Swe), and τ(P301L) transgenes (27, 28). In the present study, we used AAV9, which carries the synapsin-1 (SYN) promoter, to specifically deliver CIP to neurons of double-Tg mice that express mutant APP and PS1 (APP/PS1). CIP was expressed widely in brain areas, including the cortex and hippocampus, after intracerebroventricular (i.c.v.) infusions. Western blotting or immunohistochemistry (IHC) analyses revealed that CIP reduced τ phosphorylation, Aβ deposit, astrocytosis and microgliosis, and neuronal apoptosis. Moreover, recovered memory performance was improved and anxiety-like behavior was decreased in CIP-treated AD mice. Results suggest that selectively targeting Cdk5 by CIP is a promising strategy for the treatment of AD.

MATERIALS AND METHODS

AAV virus preparation

Myc-tagged CIP was generated by PCR by using plasmid pcDNA3.1-C-p35 as the template and was inserted in pCR2.1. Primers used included the following: 5′-TTTT*GGATCC*GCCACCATGGCATCAATGCAGAAGCTGATCTCAGAGGAC CTGATGTGCCTGGGTGAGTTTCTCTG-5′; and 3′-TTTT*TCTAGA*TTATGGGTCGGCATTTATCT-3′. *Eco*RI and *Xba*I sites are italicized, and the Myc sequence is underlined. After confirming the CIP sequence by Sanger sequencing, Myc-CIP was cut by *Eco*RI/*Xba*I and in-frame fused at the C terminus of EGF in plasmid pEGFP-C2 (Takara, Kusatsu, Japan). EGFP-myc-CIP fragment was obtained by cutting pEGFP-myc-CIP with *Age*I/*Hin*dIII, then replacing the eGFP reporter gene driven by the human SYN-1 promoter (University of Pennsylvania Vector Core Facility, Philadelphia, PA, USA). The resulting plasmid pAAV-hSYN-EGFP-CIP was transfected in human embryonic kidney 293T (HEK293T) cells, which were cultured in DMEM that was supplemented with 10% fetal bovine serum (Thermo Fisher Scientific, Waltham, MA, USA). Expression of GFP-CIP fusion protein was verified. AAV9-GFP-CIP or control AAV9-GFP was produced by Hanbio Biotechnology (Shanghai, China). In brief, HEK293T cells were transfected by Lipofiter (Hanbio Biotechnology) with 3 plasmids: pAAV-hSYN-EGFP-CIP or pAAV-hSYN-GFP, AAV helper plasmid (Hanbio Biotechnology), and pAAV2/9 containing AAV2 rep and AAV9 cap genes (Hanbio Biotechnology). At 72 h after transfection, cells were collected and lysed by using a freeze-thaw procedure. Viral particles were purified with V1369 column (Biomiga, San Diego, CA, USA). Copy numbers of vector genomes (vgs) were 2.5 or 4×10^{12} vg/ml as determined by quantitative PCR with WPRE primers: (forward) 5′-GTGCACTGTGTTTGCTGACG-3′, (reverse) 5′-GAAAGGAGCTGACAGGTGGT-3′. All AAV vectors were suspended in sterile PBS as final concentration to 10^{12} vg/ml.

I.c.v. administration of AAV virus in mice

Animal protocols were approved by the Southern Medical University Committee on Animal Care and conducted in accordance with the *Guideline for the Care and Use of Laboratory Animals* (Southern Medical University). C57BL/6J mice (male, 4–6 wk old) were purchased from the animal facility of Southern Medical University. Male APP/PS1 mice (APPswe, PSEN1dE9, 85Dbo/MmJNju mice), which express human mutant APP and PS1, were purchased from Model Animal Research Center of Nanjing University (Nanjing, China). All mice were fed in a well-ventilated, quiet room (28°C) with 12-h light/dark cycle, with access to water and food *ad libitum*. Animals received i.c.v. injection of different treatments at 3 mo old and were divided into 4 groups with 12 mice in each group: *1*) wide-type (WT) group: C57BL/6J mice with PBS injection; *2*) AD/PBS group: APP/PS1 mice with PBS injection; *3*) AD/GFP group: APP/PS1 mice with injection of AAV9-GFP; and *4*) AD/CIP group: APP/PS1 mice with injection of AAV9-GFP-CIP. All surgery procedures were conducted under aseptic conditions. Mice were anesthetized with isoflurane (4% for induction and 2% for maintenance; RWD, Shenzhen, China), mixed with oxygen (1 L/min), and delivered through a nasal mask (RWD). I.c.v. injection was conducted *via* stereotaxic apparatus (68010; RWD) according to manufacturer instructions and the atlas of mice brain (the stereotaxic coordinates were 0.5 mm posterior and 1.0 mm lateral to the bregma, and 2.5-mm deep from the dural surface) as reported (29). Infusion of 2 μl virus solution was controlled at a rate of 1 μl/min using a microinjection pump (RWD). After injection, the injection needle was maintained in place for an additional 2 min to prevent reflux.

IHC analysis and confocal microscopy

Preparation of mice brain section for IHC were performed as reported (30, 31). In brief, deeply anesthetized mice (120 mg/kg, i.p. sodium pentobarbital) were transcardially perfused with ice-cold PBS followed by 4% paraformaldehyde. Brains of 6- or 10-mo-old mice were obtained and bisected along the midline. For each mouse, one half brain sample was collected and stored at −80°C for Western blotting. Another one half was paraffin embedded and 4-μm sections were sliced with Leica RM vibratome (Leica Microsystems, Heidelberg, Germany). Antigen-retrieved sections were incubated with primary Abs overnight at 4°C. Primary Abs were goat anti-Iba1, (1:500 dilution; Thermo

Fisher Scientific), mouse anti–glial fibrillary acidic protein (GFAP) (1:1000 dilution; Millipore, Billerica, MA, USA), and mouse anti–Aβ1-42 (1:1000 dilution; Thermo Fisher Scientific). Secondary Abs SP-9001 against rabbit primary Ab and SP-9002 against mouse primary Ab were from ZSGB-BIO (Beijing, China). Activated microglial cells (stained with anti-Iba1 Ab), astrocytes (stained with anti-GFAP Ab), and senile plaques (stained with anti–Aβ1-42 Ab) were counted blindly by independent investigators. Nissel staining was performed to quantify neuronal density in sections. GFP fluorescent images were obtained with a laser scanning confocal microscope (Olympus, Tokyo, Japan). Quantitative analysis of IHC data by ImageJ software (National Institutes of Health, Bethesda, MD, USA) was double blinded.

Western blot

Western blot analysis was routinely performed as previously reported (32). All primary Abs were used at 1:1000 dilution as following: S199 (phospho-τ pSer199 Ab; Thermo Fisher Scientific), AT180 (phospho-Tau Thr231 mouse mAb; Thermo Fisher Scientific), TAU-5 (τ Ab; Thermo Fisher Scientific), mouse anti-GFAP (Millipore), AT8 (phospho-paired helical filament-τ pSer202+Thr205 mouse mAb; Thermo Fisher Scientific), goat anti-Iba1 (1:700 dilution; Thermo Fisher Scientific), rabbit cleaved caspase-3 Ab (Asp175; Gene Tex, Irvine, CA, USA), and anti–β-actin (Proteintech, Chicago, IL, USA). Secondary horseradish peroxidase–conjugated Abs were purchased from Santa Cruz Biotechnology (Santa Cruz, CA, USA) (1:1000 dilution).

Animal behavioral studies

All behavioral tests were conducted at age 6 mo. Mice were housed and habituated for 2 h in behavioral testing rooms before tests. All tests were conducted on consecutive days in a dimly illuminated room with standard conditions of temperature and free from any stray noise. All behavioral apparatus were cleaned with 75% ethanol and dried between each animal. Behavioral outcome was recorded by 2 trained assistants who were blinded to the information of each mouse.

Morris water maze

To assess spatial learning and memory, the Morris water maze (TSE Co., Thuringia, Germany) was performed according to protocol (33) with minor modifications. In brief, a circular pool (110 cm diameter, 60 cm height) was filled with water that was stirred with white dye, the temperature of which was maintained at 24–26°C. A gray curtain surrounded the pool to eliminate environmental interference. Visual cues, including a triangle figure, a square figure, and a round figure of different colors, were affixed to the curtain for memory cue. Mice were trained to find a hidden platform (8 cm diameter, 30 cm height, 1 cm below the water surface) for 4 d. In the training stage, mice were placed in the water for 60 s to find and escape onto the platform. If mice failed, they were placed on the platform for 15 s to remember the location of the platform. In the testing stage, the platform was removed and mice were monitored for a 60-s free swim in the pool. The swimming pathway was recorded by TSE video system. The latency spent in the target quadrant (the previous platform was in the quadrant) and the number of crossings of the platform position were recorded to evaluate the spatial memory of mice. All tests were performed in daytime from 9:00 AM to 3:00 PM, and animals in the 4 groups were tested alternately to minimize the impact caused by the different testing times of day.

Shuttle box active avoidance test

The shuttle box (TSE) was divided into 2 compartments of equal size (190 × 190 × 120 mm), separated by a wall that contained a hole on the bottom (8 cm in width and 10 cm in height) for mice to move 2 ways freely. Each compartment installed a lamp on the celling and the steel grid floor was connected to electricity for foot shock. Mice took 5 min to habitat the environment before the test. Once the light was on (for 10 s) in 1 compartment, the tested mouse would escape to the light compartment to avoid electric shock (for 10 s, 0.4–0.6 mA, 30-s interval). At this point, a conditional reaction (active avoidance response) would be counted. If the tested mouse stayed in the dark compartment and received the electric shock, and then went to the light compartment, an unconditional reaction would be counted. Each mouse

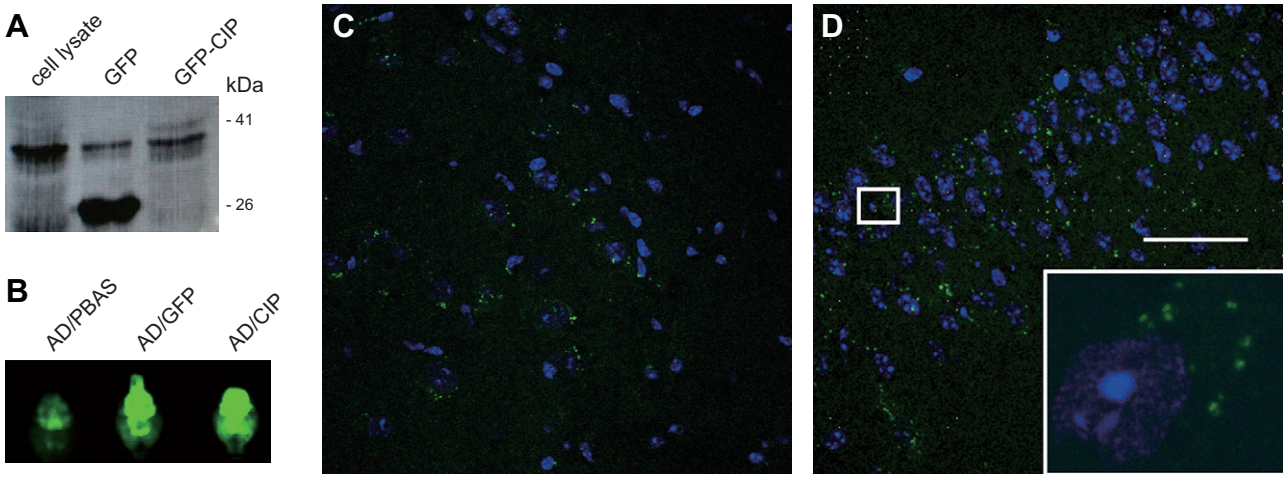

Figure 1. Distribution of AAV9-GFP-CIP after i.c.v. infusions. *A*) Expression plasmids pAAV-hSYN-GFP(GFP) and pAAV-hSYN-GFP-CIP (GFP-CIP) were transfected in HEK293 cells. Western blotting was performed for cell lysate. Arrows indicate expressed protein bands with 26 and 41 kDa for GFP and GFP-CIP, respectively. *B*) Two microliters of 10^{12} vg/ml AAV9-GFP and AAV9-GFP-CIP were i.c.v. infused in the mouse brain. One week later, mice were euthanized and brain tissue was quickly obtained to capture green fluorescence under the Kodak image machine. Obvious fluorescence was observed in the virus-injected brain, AD/GFP, and AD/CIP but not in the control AD/PBS. *C*, *D*) One week after i.c.v. virus injection, brain sections were dissected and green fluorescence was observed under confocal microscope. Green fluorescence was clearly seen in cell bodies of the cortex (*C*) or hippocampus (*D*) of AAV9-GFP-CIP–injected mice with ×600 and 2000 magnification, respectively. Scale bar, 50 μm.

conducted this test for 60 times/d on 4 consecutive days. All reactions were recorded by a TSE video and software system and the total number of active avoidance responses was analyzed.

Elevated plus maze

Elevated plus maze apparatus was made of acrylic (white) and consisted of 2 open arms (50 × 10 cm) and 2 closed arms with no roof (50 ×10 × 40 cm) at right angles to each other and an open square (10 × 10 cm) in the center. The maze was elevated 50 cm above the floor. Animals were placed in the center facing the same open arm each time. If an animal fell from the maze, it was immediately placed back in the position from which it had fallen. The duration of the elevated plus maze recording was 5 min.

Statistical analysis

Data are presented as means ± SD. Data of escape latency in the Morris water maze test and responses in the shuttle box active avoidance response test were analyzed by repeated-measures ANOVA followed by least significant difference test. All other data were analyzed by 1-way ANOVA followed by least significant difference test. Statistical analysis was performed by using SPSS version 20 (SPSS, Chicago, IL, USA). A value of $P < 0.05$ was considered statistically significant.

RESULTS

Generation of AAV9-GFP-CIP and distribution of AAV9-GFP-CIP in mice by i.c.v. injection

To generate AAV9 plasmid that expressed CIP, c-myc–tagged CIP was developed by using PCR, then C-terminally fused with EGFP in plasmid pEGFP-C2. The EGFP-myc-CIP fragment was then used to replace the eGFP reporter gene in pAAV-hSYN-GFP, which is driven by the human SYN-1 promoter, which led to expression in neurons. As shown in **Fig. 1*A***, GFP and GFP-CIP fusion proteins were evidently expressed after transfection of pAAV-hSYN-GFP and pAAV-hSYN-GFP-CIP, respectively, in HEK293T cells. In *in vivo* imaging, GFP was remarkably expressed in the brain of mice 1 wk after i.c.v. infusion of purified AAV9-GFP and AAV9-GFP-CIP vectors, but not AD/PBS as control (Fig. 1*B*). To further assess the distribution of viruses in the brain, green fluorescence of brain sections was observed using confocal microscopy. As shown in Fig. 1*C*, *D*, GFP was expressed in cell bodies of the mouse cerebral cortex (Fig. 1*C*) and hippocampus (Fig. 1*D*) after AAV9-GFP-CIP infusions, which indicated the expression of

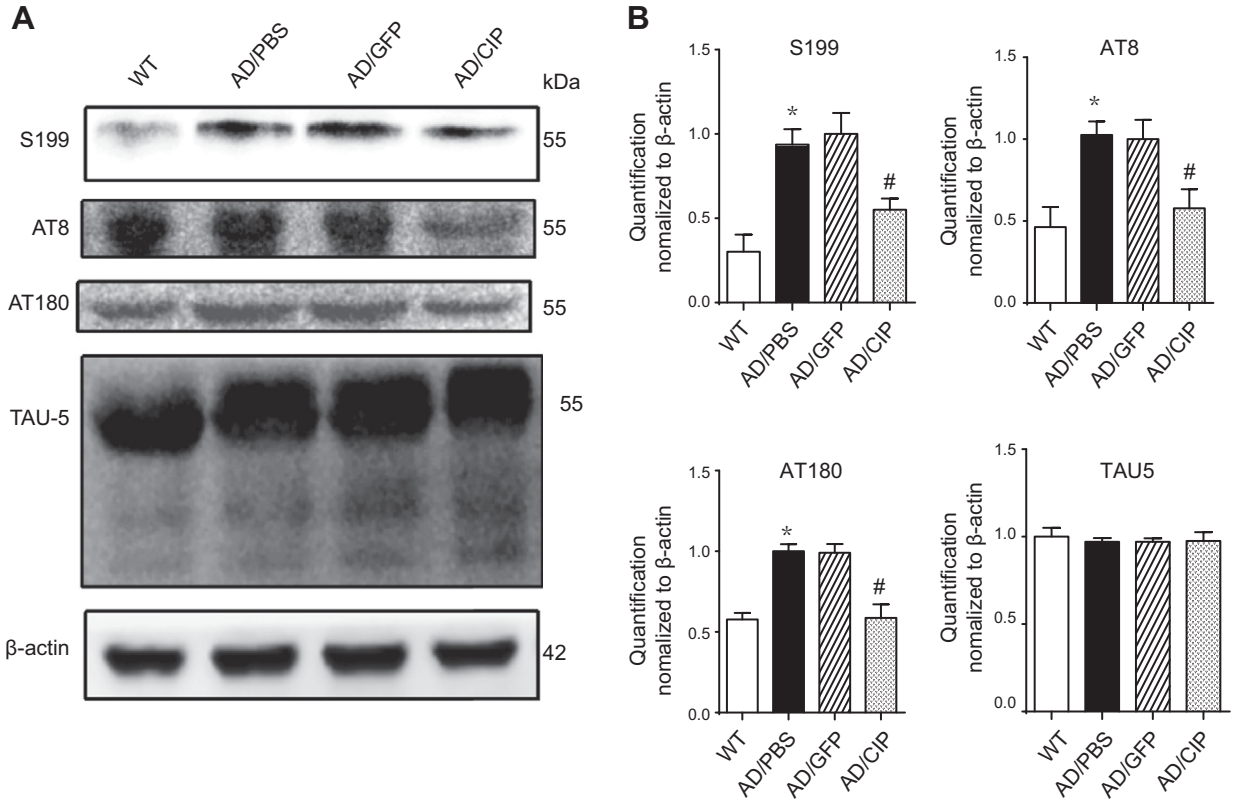

Figure 2. AAV9-GFP-CIP reduced τ phosphorylation in AD mice. Two microliters of 10^{12} vg/ml AAV9-GFP or AAV9-GFP-CIP virus were i.c.v. injected in APP/PS1 mice at age 3 mo, and i.c.v. injection of PBS in AD or WT mice were controls. Six months later, brain samples were obtained to check τ phosphorylation by Western blotting. *A*) For Western blotting results, τ phosphorylation was tested at the following sites: Ser199 by S199 Ab, Ser202 and Thr205 by AT8 Ab, and Thr231 by AT180 Ab. Increased τ phosphorylation was observed at all these sites in AD mice (AD/PBS), which was decreased in AAV9-GFP-CIP–treated mice (AD/CIP) but not in AAV9-GFP–treated mice (AD/GFP). Total τ was tested by anti-TAU5 Ab. There was no significant difference among 4 groups. *B*) Relative intensities of τ levels normalized to β-actin. Comparing the summarized data of 3 tests for each group, there were more τ phosphorylation sites detected by anti-Ser199, AT180, and AT8 Abs in AD mice (AD/PBS) than in WT mice ($^{*}P < 0.05$), and less in AAV9-GFP-CIP–treated mice (AD/CIP) than in AD mice ($^{\#}P < 0.05$). No difference was found between AD and AAV9-GFP group.

GFP-CIP fusion protein. Thus, results demonstrate the successful generation of AAV9-GFP-CIP, which is able to deliver GFP-CIP in brain cells in mice.

AAV9-GFP-CIP reduced hyperphosphorylation of τ in APP/PS1 mice

Hyperphosphorylation of τ at multiple sites contributes to the formation of PHF in NFTs, one of the hallmarks of AD (34–36). Previous studies have demonstrated that aberrant Cdk5/p25 increases phosphorylated τ of PHF at multiple sites in the brain of 3×AD, 5×FAD, and p25-Tg mice (3, 28, 37). In the present study, we assessed whether 1 dose of AAV9-GFP-CIP *via* i.c.v. infusions in 3-mo-old APP1/PS1 mice would inhibit τ phosphorylation when tested at 6 mo old when behavior deficits would be observed. As shown in **Fig. 2*A***, Western blot analysis revealed that τ phosphorylation was increased in AD control mice at the following sites: Ser199 tested by S199 Abs, Ser202 and Thr205 by AT8 Abs, and Thr231 by AT180 Abs. Quantified levels of protein bands against β-actin are presented in Fig. 2*B*. Treatment with AAV9-GFP-CIP, but not AAV9-GFP (control), decreased hyperphosphorylation of τ. There was no difference in total τ (TAU5) among groups. Data demonstrate that administration of AAV9-GFP-CIP after the onset of pathogenesis in AD mice reduces phosphorylation of τ.

AAV9-GFP-CIP reduced Aβ aggregation in APP/PS1 mice

Aβ deposition—the primary pathogenesis of AD—occurs as early as 8 wk in APP/PS1 mice (38). As shown in **Fig. 3*A*** and quantified in Fig. 3*B*, gradually increased Aβ deposition was observed in the cerebral cortex and hippocampus of APP/PS1 mice at 6 mo (Fig. 3*A*) and 10 mo. Of importance, 1 dose of AAV-CIP administered at 3 mo before marked behavioral changes significantly decreased the number and size of the deposition of Aβ peptide at 6 and 10 mo. In contrast, treatment with AAV9-GFP (control) had no effect.

AAV9-GFP-CIP reduced inflammation and apoptosis

Neuroinflammation is the common feature of neurodegenerative diseases, in which activated astrocytes and microglia play a major role (39). In the present study, we examined inflammation status by using Western blotting at 6 mo old, and IHC analysis at 6 and 10 mo old. **Figure 4*A*** shows the IHC data of mice at 6 and 10 mo old. Astrocyte activation in the brain of AD mice was obvious at 6 mo old and significantly increased at 10 mo old, as indicated by GFAP staining. Similarly, microgliosis was observed as staining by anti-Iba1 Ab. Western blot analysis also confirmed the increased level of Iba1 in AD mouse brain at 6 mo old (Fig. 4*B*). Quantification of images demonstrated that AAV9-GFP-CIP significantly reduced the levels of GFAP and Iba1 compared with AAV9-GFP or PBS control (Fig. 4*D*, *E*).

Loss of neurons is also a feature of AD. As shown in **Fig. 5*B***, apoptosis was robust as indicated by the increased levels of cleaved caspase- 3; this was decreased by AAV9-GFP-CIP, but not AAV9-GFP (Fig. 5*D*). However, different from 5×FAD and p25-Tg mice, neural loss and brain atrophy were not observed at the time point examined, regardless of treatment (Fig. 5*C*, *E*, *F*, data at 6 mo old; similar data were not shown at age 10 mo). In APP/PS1 mice, neuronal loss appears in the brain area with high neuron density at older ages (*e.g.*, age 17 mo) (40).

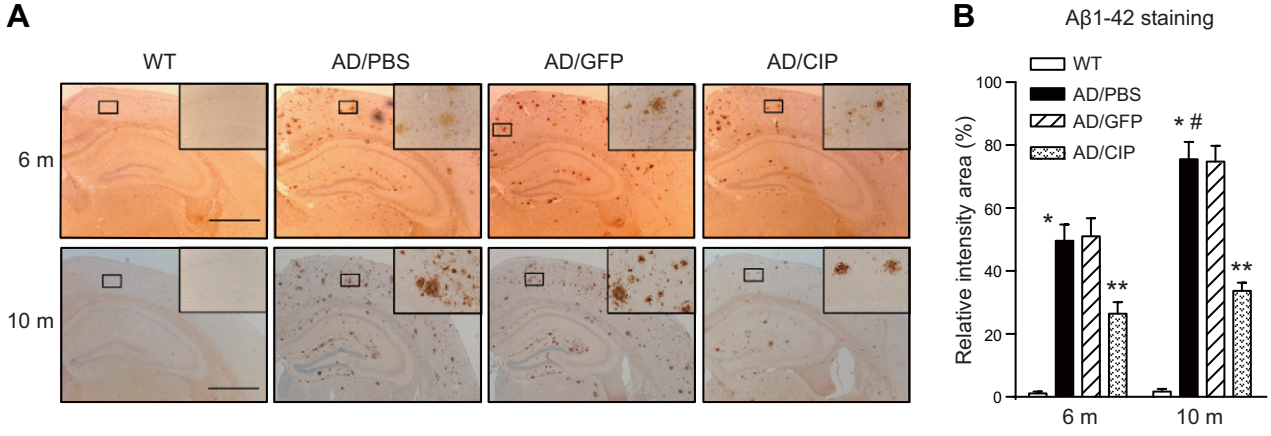

Figure 3. Aβ aggregation in AD mice was reduced by CIP treatment. Paraffin-embedded brain sections were prepared from 6- or 10-mo-old mice that had underwent different treatments for 3 or 7 mo. *A*) Aβ1-42 staining showed marked Aβ aggregation in the cortex and hippocampus area in AD mice at age 6 or 10 mo, as shown in ×40 and 200 magnification. AAV9-GFP-CIP, but not AAV9-GFP, treatment reduced numbers of Aβ deposit. Scale bars, 1 mm. *B*) Numbers of Aβ plaque were counted in 3 slices. There were prominent Aβ numbers in AD mice compared with WT mice, which were significantly increased at age 10 mo. Three months of treatment of AAV9-GFP-CIP, but not AAV9-GFP, ameliorated Aβ aggregation in AD mice (AD/CIP). The treatment effect of AAV9-GFP-CIP lasted for 7 mo as the end point of the study (AD/CIP). $^{*}P < 0.05$ compared with WT mice; $^{**}P < 0.05$ compared with AD mice; $^{\#}P < 0.05$, comparing 10- and 6-mo-old mice.

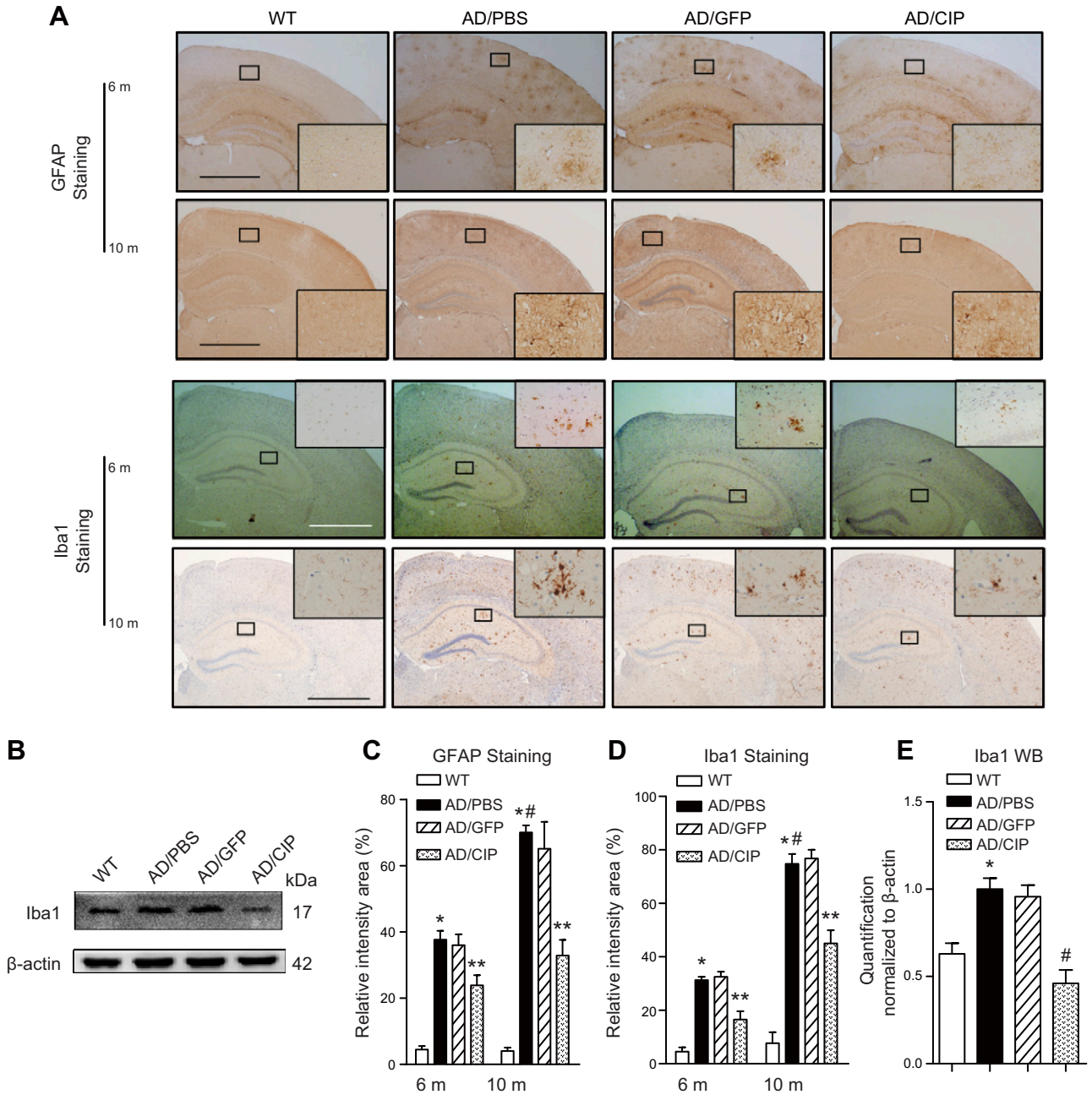

Figure 4. Inflammation was alleviated in AAV9-GFP-CIP–treated AD mice. Inflammation was assessed in brain sections of AD mice at age 6 and 10 mo (showed as 6 or 10 m). *A*) IHC staining by anti-GFAP Ab and Iba1 Ab for assessing activation of astrocytes and microgliocytes, respectively, with ×40 and 200 magnification. Scale bars, 1 mm. *B*) Microgliosis was also analyzed in brain tissues at age 6 mo by Western blotting (WB) with anti-Iba1 Ab. *C*, *D*) Numbers of staining cells counted in 3 slices for GFAP (*C*) and Iba1 (*D*) staining, respectively. In AD mice (AD/PBS), activation of astrocytes and microcytes was obvious at age 6 mo ($^{*}P < 0.05$, compared with WT mice), which was significantly increased at age 10 mo. $^{\#}P < 0.05$, comparing 10 and 6 mo. AAV9-GFP-CIP treatment remarkably reduced inflammation at 6 and 10 mo checked points. $^{**}P < 0.05$, compared with AD/PBS or AD/GFP. *E*) Relative intensities of Iba1 levels normalized to β-actin. Iba1 level was increased in AD mice and decreased in CIP treated mice. $^{*}P < 0.05$, AD mice compared with WT mice. $^{\#}P < 0.05$, AAV9-GFP-CIP–treated mice compared with AD mice.

AAV9-GFP-CIP rescued learning and memory deficits and decreased anxiety-like behavior in AD mice

To determine whether AAV9-GFP-CIP treatment rescued the neuropathologic changes, apoptosis, and behavioral deficits, APP/PS1 transgenic mice at 6 mo old were tested for memory and anxiety-like behavior by using the Morris water maze and the shuttle box active avoidance tests, and elevated plus maze test, respectively.

The Morris water maze test was carried out on 5 consecutive days to measure hippocampal-dependent memory (41, 42). WT mice took less time to reach the hidden platform over the 4-d training trials, whereas AD mice that were treated with PBS vehicle (AD/PBS) or AAV9-GFP (AD/GFP) spent a longer time, in particular,

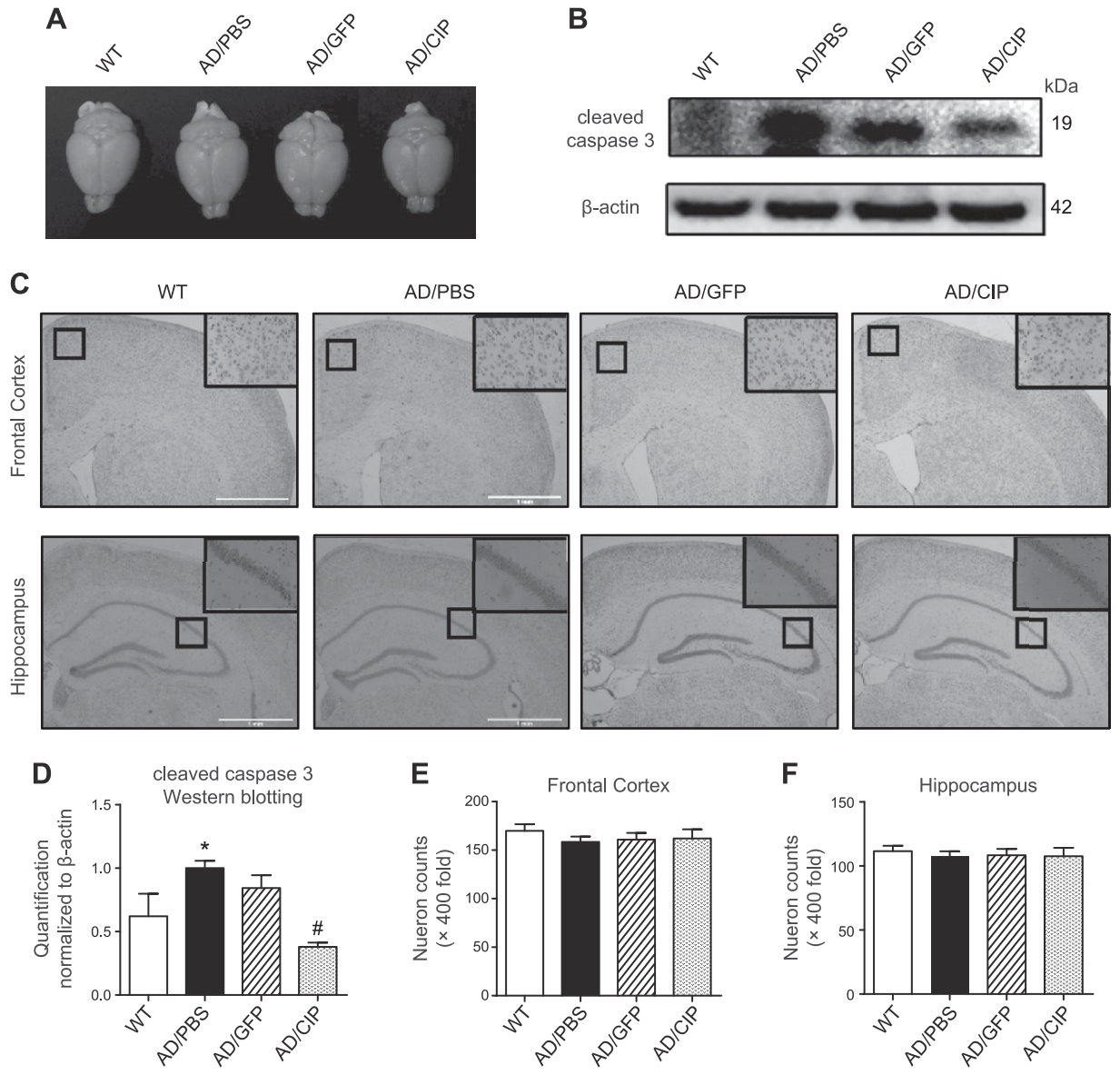

Figure 5. AAV9-GFP-CIP treatment reduced apoptosis in AD mice. Mice in 4 groups were euthanized at 6 mo after 3 mo of treatment. *A*) There was no difference in brain size among the different groups. *B*) Western blotting of cleaved caspase-3 of freshly distracted mice brain to measure apoptosis. *C*) Nissl staining. Frontal cortex (upper panel) and hippocampus (lower panel). The lower magnification showed ×40-fold, and the higher magnification showed ×400-fold. Scale bars, 1 mm. *D*) Relative intensity of cleaved caspase-3 bands normalized to β-actin. Cleaved caspase-3 level was increased in AD mice, and decreased in CIP treated mice. $^{*}P < 0.05$, AD mice compared with WT mice, $^{\#}P < 0.05$, AAV9-GFP-CIP–treated mice compared with AD mice. *E*, *F*) Neuronal counts of frontal cortex (*E*) and hippocampus (*F*), ×400 magnification. There was no significant difference among 4 groups.

on d 3 and 4. In contrast, mice that were treated with AAV9-GFP-CIP (AD/CIP) displayed recovered latency that was close to WT levels (**Fig. 6*A***). During the probe trail test on d 5 when the previous platform was removed, AAV9-GFP-CIP–treated mice spent more time in the target quadrant compared with AD mice that were treated with PBS or AAV9-GFP ($P < 0.05$), which spent less time in the target quadrant compared with WT mice ($P < 0.05$; Fig. 6*B*). Similarly, WT and AAV9-GFP-CIP–treated AD mice crossed more times around the target quadrant than did AD mice that were treated with PBS or AAV-GFP ($P < 0.05$), which suggested the reversal by CIP of memory deficits in AD mice.

The shuttle box active avoidance test was used to assess the learning ability of the mice. As shown in Fig. 6*D*, AD/PBS mice and AD/GFP mice displayed significant impairment of active avoid response since d 1. In contrast, AAV9-GFP-CIP–treated mice (AD/CIP) tended to recover the response on d 3 and displayed significant recovery on d 4 ($P < 0.05$).

Anxiety commonly occurs in patients with AD, and anxiety-like behavior is another phenotype of AD mice (43, 44). As shown in the elevated plus maze test (Fig. 6*E*, F), AD mice that were treated with PBS (AD/PBS) or AAV9-GFP (AD/GFP) spent less time and had fewer entries in the open arms compared with WT controls ($P < 0.05$). In

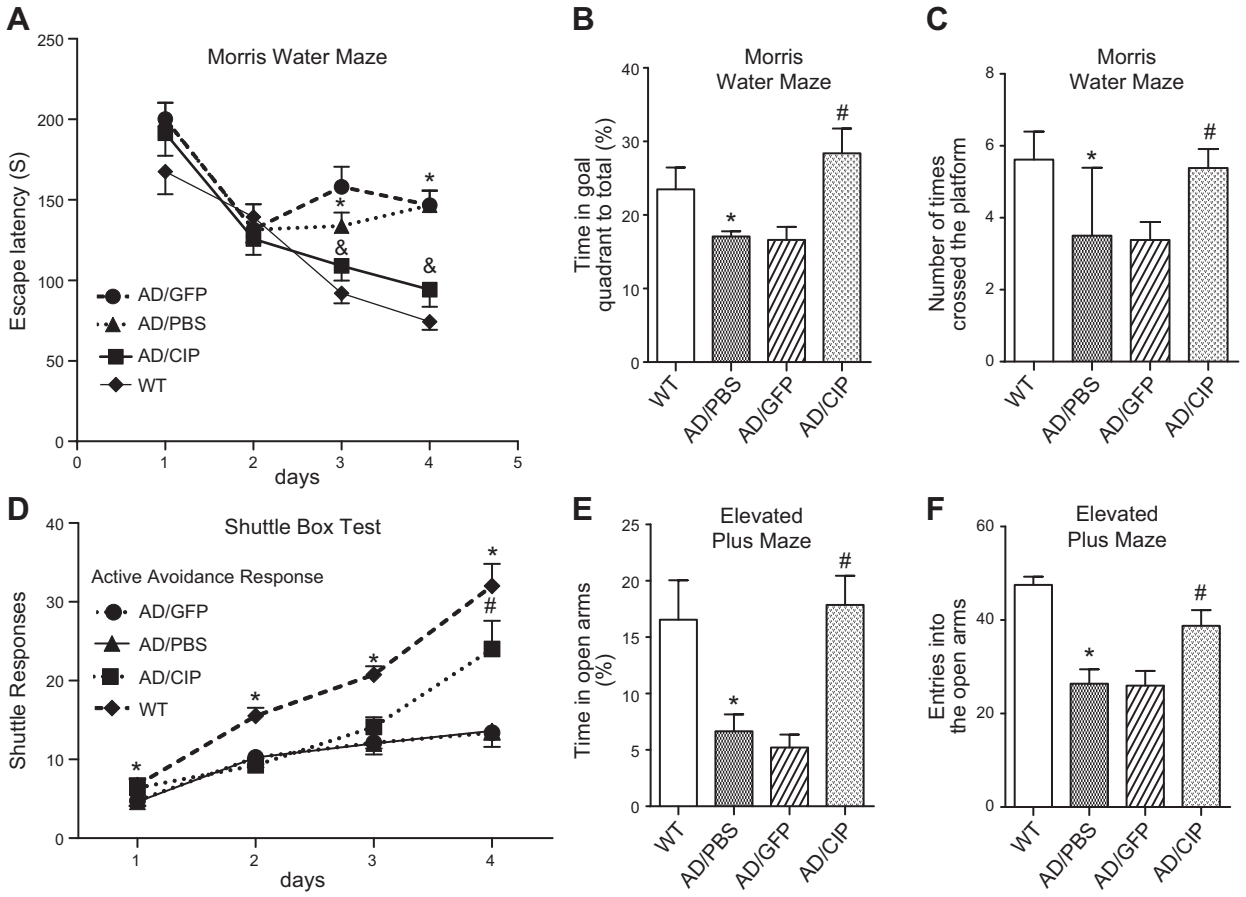

Figure 6. Memory deficit and anxiety in AD mice were alleviated by treatment with AAV9-GFP-CIP. Behavioral studies were performed in animals at age 6 mo after 3 mo of AAV treatment, including Morris water maze and shuttle box active avoidance test for memory assessment, and elevated plus maze for anxiety. Eight mice were used for each group. *A–C*) Morris water maze test. *A*) In the 4 d of training, AD mice showed longer escape latency compared with WT. $^{*}P < 0.05$. However, mice in AAV9-GFP-CIP groups markedly recovered the escape latency close to the WT level. $P < 0.05$. AAV9-GFP control had no effect. *B*) When the platform was moved away at d 5, AD mice spent less time in the goal quadrant compared with WT. $^{*}P < 0.05$. AAV9-GFP-CIP, but not AAV9-GFP, increased the consumed time to WT level. $^{\#}P < 0.05$ compared with AD mice. Similar results were observed for the number of times the mice crossed the previous platform as in panel *C*. *D*) Shuttle box active avoidance response test. AD mice showed slow response compared with WT. $^{*}P < 0.05$, which was significantly recovered by treatment with AAV9-GFP-CIP but not AAV9-GFP. $^{\#}P < 0.05$. *E, F*) In elevated plus maze test, AD mice entered (*F*) and spent less time (*E*) in the open arms compared with WT mice. $^{*}P < 0.05$. Conversely, AAV9-GFP-CIP–treated AD mice had similar numbers or time spent in the open arms compared with WT mice. $^{\#}P < 0.05$ compared with AD mice, which was not observed in AAV9-GFP–treated mice.

contrast, AD mice that were treated with AAV9-GFP-CIP (AD/CIP) showed significant increases in both indexes compared with AD/PBS or AD/GFP ($P < 0.05$).

Taken together, these results suggest that CIP reverses cognitive deficits and anxiety-like behavior in AD mice.

DISCUSSION

Cdk5/p35 activity has been well documented in the role of neuronal functions (4–6), whereas aberrant Cdk5/p25 activity contributes to the pathogenesis of several degenerative diseases, including AD (8, 9). Selectively targeting on activity of Cdk5/p35 other than Cdk5/p35 is preferred to avoid adverse effects. Targeting aberrantly hyperactive Cdk5 selectively *in vivo* has been successful in APP/PS1 mice by TFP5 and p25-Tg mice by genetic overexpression of CIP. In the present study, CIP was successfully delivered to cerebral neurons of APP/PS1-Tg mice by i.c.v. infusions of AAV-9 vectors that expressed CIP. AAV9-GFP-CIP reduced hyperphosphorylation of τ protein and aggregation of Aβ peptide, alleviated microgliosis and astrocytosis, reduced apoptosis, recovered cognitive function, and decreased anxiety in AD mice after 3- or 7-mo treatment. Our results therefore provide additional evidence that CIP prevents pathogenetic changes that are caused by Cdk5 dysfunction and that selective inhibition of Cdk5 is a practical strategy for treatment of AD.

In the present study, we demonstrated that selectively targeting Cdk5 by CIP in the brain of APP/PS1 mice after onset of pathogenetic alteration reversed most of the pathologic and behavioral phenotypes. Previous studies in APP/PS1-Tg mice have demonstrated that Aβ accumulation is the primary pathologic change in the cerebral cortex, occurring as early as age 8 wk, whereas hyperphosphorylation of τ presents around Aβ deposits in the

cerebral cortex and hippocampus at 24 wk of age (38). To determine the effect of CIP after the occurrence of Aβ deposits and tauopathy, we injected AAV-CIP once *via* i.c.v. in APP/PS1 mice at age 3 mo. Our data indicate that AAV-GFP-CIP administered after onset of pathogenesis reduced amyloid and τ pathologies as well as neuroinflammation at age 6 mo in APP/PS1 mice. Continuing neuroprotection lasted to age 10 mo, when the study ended. Similarly, treatment of TFP5 significantly rescued AD pathology in 5×FAD mice (3); however, it will be inconvenient to inject repeatedly for long-term treatment. In the CIP genetic intervention study, CIP treatment existed before the induced expression of p25 (18), which demonstrates the preventive effect of Cdk5 inhibition. Consistent with our study, shCDK5miR delivered by AAV5 in the hippocampus after onset of symptoms at age 6 mo reversed τ aggregation and prevented spatial memory impairment (28). Because neuropathogenic changes in AD are prominent firstly in the hippocampus, then progressively occurred in other brain areas, thus, i.c.v. infusions instead of infusions into specific brain regions, such as the hippocampus, would be a better delivery way to cover more brain areas. Indeed, CIP was successfully delivered by AAV9 into cells of the cerebral cortex and hippocampus, as indicated by GFP expression. Taken together, our study and others demonstrated that targeting Cdk5 is effective in the prevention of and reversal of pathologic changes, which eventually benefits behavioral recovery. In addition, using the AAV virus system to deliver selective inhibitors of Cdk5 is more practical than engineering peptides as a result of the 1-dose injection with long-term protection and the flexibility of injection time and location.

Although there are some disputes around the role of p25 in the development of AD-like pathology (45–47), more studies support the contribution of Cdk5/p25 to the development of AD. p25-Tg mice with p25 overexpression display a robust increase in Cdk5 activity, which leads to phosphorylated τ and neuronal death *in vivo* (9, 31, 48). APP/PS1 mice primarily exhibit the burden of Aβ and then tauopathy. It is noted that p25 accelerates AD pathogenesis by enhancing BACE1 activity *via* phosphorylation (49). Although we did not observe the obvious expression of p25 in the whole brain of APP/PS1 mice at age 7 mo (data not shown), hyperphosphorylation of τ was reduced at Cdk5-specific sites [*i.e.*, Ser202 and Thr205 (AT-8), which are related to aging, or PHF in PS1 KI mice] (38). Of interest, CIP clearly reduced but did not abolish Aβ plaques. Inflammation, which is a causative factor throughout AD development, was also significantly reduced. Moreover, Cdk5 inhibition produced alleviation of pathogenesis and the reversal of behavioral deficits. The study in p25-Tg and AD mice with 3 different treatments further provides evidence for the dysfunction of p25 in the development of an AD-like phenotype.

Overall, the results in our study demonstrated the feasibility of using AAV9-GFP-CIP to target Cdk5 and reduce its hyperactivity. CIP can be used for the treatment of AD. Further studies are needed to determine the long-term effect and survival rate in AD mice after AAV9-GFP-CIP treatment. Synaptic activities (LTP/LDP) related to learning and restoring memory or Cdk5 activities among different groups have not been performed in the present study because of the lack of equipment or certification of radioactive material, respectively, which are undertaken in future studies. FJ

ACKNOWLEDGMENTS

This work was supported by the National Nature Science Fund of China (Grant 81271430) and Guangdong Provincial Universities fund (2012-328) for Experts Recruitment Program (to Y.H.). A patent application (HX2016-187) has been filed regarding AAV9-GFP-CIP as a potential therapeutic method for AD.

AUTHOR CONTRIBUTIONS

S. Pan and Y. Hu designed the study; Y. He performed experiments; M. Xu and W. Huang performed the IHC experiment; R. He performed i.c.v. injections; J. Huang constructed AAV expression plasmids; W. Huang and P. Song performed animal behavioral studies; R. He and W. Huang analyzed data; H.-T. Zhang supervised animal behavioral studies and revised the manuscript; and Y. Hu wrote the paper.

REFERENCES

1. Ballatore, C., Lee, V. M., and Trojanowski, J. Q. (2007) Tau-mediated neurodegeneration in Alzheimer's disease and related disorders. *Nat. Rev. Neurosci.* **8**, 663–672
2. Shukla, V., Mishra, S. K., and Pant, H. C. (2011) Oxidative stress in neurodegeneration. *Adv. Pharmacol. Sci.* **2011**, 572634
3. Shukla, V., Zheng, Y. L., Mishra, S. K., Amin, N. D., Steiner, J., Grant, P., Kesavapany, S., and Pant, H. C. (2013) A truncated peptide from p35, a Cdk5 activator, prevents Alzheimer's disease phenotypes in model mice. *FASEB J.* **27**, 174–186
4. Su, S. C., and Tsai, L. H. (2011) Cyclin-dependent kinases in brain development and disease. *Annu. Rev. Cell Dev. Biol.* **27**, 465–491
5. Nikolic, M., Dudek, H., Kwon, Y. T., Ramos, Y. F., and Tsai, L. H. (1996) The cdk5/p35 kinase is essential for neurite outgrowth during neuronal differentiation. *Genes Dev.* **10**, 816–825
6. Ohshima, T., Ward, J. M., Huh, C. G., Longenecker, G., Veeranna, Pant, H. C., Brady, R. O., Martin, L. J., and Kulkarni, A. B. (1996) Targeted disruption of the cyclin-dependent kinase 5 gene results in abnormal corticogenesis, neuronal pathology and perinatal death. *Proc. Natl. Acad. Sci. USA* **93**, 11173–11178
7. Patrick, G. N., Zukerberg, L., Nikolic, M., de la Monte, S., Dikkes, P., and Tsai, L. H. (1999) Conversion of p35 to p25 deregulates Cdk5 activity and promotes neurodegeneration. *Nature* **402**, 615–622
8. Ahlijanian, M. K., Barrezueta, N. X., Williams, R. D., Jakowski, A., Kowsz, K. P., McCarthy, S., Coskran, T., Carlo, A., Seymour, P. A., Burkhardt, J. E., Nelson, R. B., and McNeish, J. D. (2000) Hyperphosphorylated tau and neurofilament and cytoskeletal disruptions in mice overexpressing human p25, an activator of cdk5. *Proc. Natl. Acad. Sci. USA* **97**, 2910–2915
9. Cruz, J. C., Tseng, H. C., Goldman, J. A., Shih, H., and Tsai, L. H. (2003) Aberrant Cdk5 activation by p25 triggers pathological events leading to neurodegeneration and neurofibrillary tangles. *Neuron* **40**, 471–483
10. Qu, D., Rashidian, J., Mount, M. P., Aleyasin, H., Parsanejad, M., Lira, A., Haque, E., Zhang, Y., Callaghan, S., Daigle, M., Rousseaux, M. W., Slack, R. S., Albert, P. R., Vincent, I., Woulfe, J. M., and Park, D. S. (2007) Role of Cdk5-mediated phosphorylation of Prx2 in MPTP toxicity and Parkinson's disease. *Neuron* **55**, 37–52
11. Nguyen, M. D., Larivière, R. C., and Julien, J. P. (2001) Deregulation of Cdk5 in a mouse model of ALS: toxicity alleviated by perikaryal neurofilament inclusions. *Neuron* **30**, 135–147

12. Smith, P. D., Crocker, S. J., Jackson-Lewis, V., Jordan-Sciutto, K. L., Hayley, S., Mount, M. P., O'Hare, M. J., Callaghan, S., Slack, R. S., Przedborski, S., Anisman, H., and Park, D. S. (2003) Cyclin-dependent kinase 5 is a mediator of dopaminergic neuron loss in a mouse model of Parkinson's disease. *Proc. Natl. Acad. Sci. USA* **100**, 13650–13655
13. Menn, B., Bach, S., Blevins, T. L., Campbell, M., Meijer, L., and Timsit, S. (2010) Delayed treatment with systemic (S)-roscovitine provides neuroprotection and inhibits *in vivo* CDK5 activity increase in animal stroke models. *PLoS One* **5**, e12117
14. Glicksman, M. A., Cuny, G. D., Liu, M., Dobson, B., Auerbach, K., Stein, R. L., and Kosik, K. S. (2007) New approaches to the discovery of cdk5 inhibitors. *Curr. Alzheimer Res.* **4**, 547–549
15. Helal, C. J., Kang, Z., Lucas, J. C., Gant, T., Ahlijanian, M. K., Schachter, J. B., Richter, K. E., Cook, J. M., Menniti, F. S., Kelly, K., Mente, S., Pandit, J., and Hosea, N. (2009) Potent and cellularly active 4-aminoimidazole inhibitors of cyclin-dependent kinase 5/p25 for the treatment of Alzheimer's disease. *Bioorg. Med. Chem. Lett.* **19**, 5703–5707
16. Zheng, Y. L., Kesavapany, S., Gravell, M., Hamilton, R. S., Schubert, M., Amin, N., Albers, W., Grant, P., and Pant, H. C. (2005) A Cdk5 inhibitory peptide reduces tau hyperphosphorylation and apoptosis in neurons. *EMBO J.* **24**, 209–220
17. Zheng, Y. L., Li, B. S., Amin, N. D., Albers, W., and Pant, H. C. (2002) A peptide derived from cyclin-dependent kinase activator (p35) specifically inhibits Cdk5 activity and phosphorylation of tau protein in transfected cells. *Eur. J. Biochem.* **269**, 4427–4434
18. Sundaram, J. R., Poore, C. P., Sulaimee, N. H., Pareek, T., Asad, A. B., Rajkumar, R., Cheong, W. F., Wenk, M. R., Dawe, G. S., Chuang, K. H., Pant, H. C., and Kesavapany, S. (2013) Specific inhibition of p25/Cdk5 activity by the Cdk5 inhibitory peptide reduces neurodegeneration *in vivo*. *J. Neurosci.* **33**, 334–343
19. Binukumar, B. K., Shukla, V., Amin, N. D., Grant, P., Bhaskar, M., Skuntz, S., Steiner, J., and Pant, H. C. (2015) Peptide TFP5/TP5 derived from Cdk5 activator P35 provides neuroprotection in the MPTP model of Parkinson's disease. *Mol. Biol. Cell* **26**, 4478–4491
20. Zhang, Q., Xie, H., Ji, Z., He, R., Xu, M., He, Y., Huang, J., Pan, S., and Hu, Y. (2016) Cdk5/p25 specific inhibitory peptide TFP5 rescues the loss of dopaminergic neurons in a sub-acute MPTP induced PD mouse model. *Neurosci. Lett.* **632**, 1–7
21. Merkel, S. F., Andrews, A. M., Lutton, E. M., Mu, D., Hudry, E., Hyman, B. T., Maguire, C. A., and Ramirez, S. H. (2017) Trafficking of AAV vectors across a model of the blood-brain barrier; a comparative study of transcytosis and transduction using primary human brain endothelial cells. *J. Neurochem.* **140**, 216–230
22. Dashkoff, J., Lerner, E. P., Truong, N., Klickstein, J. A., Fan, Z., Mu, D., Maguire, C. A., Hyman, B. T., and Hudry, E. (2016) Tailored transgene expression to specific cell types in the central nervous system after peripheral injection with AAV9. *Mol. Ther. Methods Clin. Dev.* **3**, 16081
23. Gonçalves, M. A. (2005) Adeno-associated virus: from defective virus to effective vector. *Virol. J.* **2**, 43
24. Gérard, C., Xiao, X., Filali, M., Coulombe, Z., Arsenault, M., Couet, J., Li, J., Drolet, M. C., Chapdelaine, P., Chikh, A., and Tremblay, J. P. (2014) An AAV9 coding for frataxin clearly improved the symptoms and prolonged the life of Friedreich ataxia mouse models. *Mol. Ther. Methods Clin. Dev.* **1**, 14044
25. Zhao, C., Qiao, C., Tang, R. H., Jiang, J., Li, J., Martin, C. B., Bulaklak, K., Li, J., Wang, D. W., and Xiao, X. (2015) Overcoming insulin insufficiency by forced follistatin expression in beta-cells of db/db mice. *Mol. Ther.* **23**, 866–874
26. Weinberg, M. S., Samulski, R. J., and McCown, T. J. (2013) Adeno-associated virus (AAV) gene therapy for neurological disease. *Neuropharmacology* **69**, 82–88
27. Oddo, S., Caccamo, A., Shepherd, J. D., Murphy, M. P., Golde, T. E., Kayed, R., Metherate, R., Mattson, M. P., Akbari, Y., and LaFerla, F. M. (2003) Triple-transgenic model of Alzheimer's disease with plaques and tangles: intracellular Abeta and synaptic dysfunction. *Neuron* **39**, 409–421
28. Castro-Alvarez, J. F., Uribe-Arias, S. A., Kosik, K. S., and Cardona-Gómez, G. P. (2014) Long- and short-term CDK5 knockdown prevents spatial memory dysfunction and tau pathology of triple transgenic Alzheimer's mice. *Front. Aging Neurosci.* **6**, 243
29. Paxinos, G., and Franklin, K. B. J. (2001) *The Mouse Brain in Stereotaxic Coordinates*, 2nd ed., Academic Press, San Diego, CA, USA
30. Zhou, X., Huang, J., Pan, S., Xu, M., He, R., Ji, Z., and Hu, Y. (2016) Neurodegeneration-like pathological and behavioral changes in an AAV9-mediated p25 overexpression mouse model. *J. Alzheimers Dis.* **53**, 843–855
31. Sundaram, J. R., Chan, E. S., Poore, C. P., Pareek, T. K., Cheong, W. F., Shui, G., Tang, N., Low, C. M., Wenk, M. R., and Kesavapany, S. (2012) Cdk5/p25-induced cytosolic PLA2-mediated lysophosphatidylcholine production regulates neuroinflammation and triggers neurodegeneration. *J. Neurosci.* **32**, 1020–1034
32. Huang, K., Gu, Y., Hu, Y., Ji, Z., Wang, S., Lin, Z., Li, X., Xie, Z., and Pan, S. (2015) Glibenclamide improves survival and neurologic outcome after cardiac arrest in rats. *Crit. Care Med.* **43**, e341–e349
33. Zhang, H. T., Huang, Y., Masood, A., Stolinski, L. R., Li, Y., Zhang, L., Dlaboga, D., Jin, S. L., Conti, M., and O'Donnell, J. M. (2008) Anxiogenic-like behavioral phenotype of mice deficient in phosphodiesterase 4B (PDE4B). *Neuropsychopharmacol.* **33**, 1611–1623
34. Grundke-Iqbal, I., Iqbal, K., Tung, Y. C., Quinlan, M., Wisniewski, H. M., and Binder, L. I. (1986) Abnormal phosphorylation of the microtubule-associated protein tau (tau) in Alzheimer cytoskeletal pathology. *Proc. Natl. Acad. Sci. USA* **83**, 4913–4917
35. Kosik, K. S., Joachim, C. L., and Selkoe, D. J. (1986) Microtubule-associated protein tau (tau) is a major antigenic component of paired helical filaments in Alzheimer disease. *Proc. Natl. Acad. Sci. USA* **83**, 4044–4048
36. Lee, V. M., Balin, B. J., Otvos, L., Jr., and Trojanowski, J. Q. (1991) A68: a major subunit of paired helical filaments and derivatized forms of normal Tau. *Science* **251**, 675–678
37. Zou, D., Zhou, Y., Liu, L., Dong, F., Shu, T., Zhou, Y., Tsai, L. H., and Mao, Y. (2016) Transient enhancement of proliferation of neural progenitors and impairment of their long-term survival in p25 transgenic mice. *Oncotarget* **7**, 39148–39161
38. Kurt, M. A., Davies, D. C., Kidd, M., Duff, K., and Howlett, D. R. (2003) Hyperphosphorylated tau and paired helical filament-like structures in the brains of mice carrying mutant amyloid precursor protein and mutant presenilin-1 transgenes. *Neurobiol. Dis.* **14**, 89–97
39. Markiewicz, I., and Lukomska, B. (2006) The role of astrocytes in the physiology and pathology of the central nervous system. *Acta Neurobiol. Exp. (Warsz.)* **66**, 343–358
40. Rupp, N. J., Wegenast-Braun, B. M., Radde, R., Calhoun, M. E., and Jucker, M. (2011) Early onset amyloid lesions lead to severe neuritic abnormalities and local, but not global neuron loss in APPPS1 transgenic mice. *Neurobiol. Aging* **32**, 2324.e1–2324.e6
41. Morris, R. (1984) Developments of a water-maze procedure for studying spatial learning in the rat. *J. Neurosci. Methods* **11**, 47–60
42. Remondes, M., and Schuman, E. M. (2004) Role for a cortical input to hippocampal area CA1 in the consolidation of a long-term memory. *Nature* **431**, 699–703
43. Mah, L., Binns, M. A., and Steffens, D. C.; Alzheimer's Disease Neuroimaging Initiative. (2015) Anxiety symptoms in amnestic mild cognitive impairment are associated with medial temporal atrophy and predict conversion to Alzheimer disease. *Am. J. Geriatr. Psychiatry* **23**, 466–476
44. Lok, K., Zhao, H., Zhang, C., He, N., Shen, H., Wang, Z., Zhao, W., and Yin, M. (2013) Effects of accelerated senescence on learning and memory, locomotion and anxiety-like behavior in APP/PS1 mouse model of Alzheimer's disease. *J. Neurol. Sci.* **335**, 145–154
45. Kerokoski, P., Suuronen, T., Salminen, A., Soininen, H., and Pirttilä, T. (2001) The levels of cdk5 and p35 proteins and tau phosphorylation are reduced during neuronal apoptosis. *Biochem. Biophys. Res. Commun.* **280**, 998–1002
46. Takashima, A., Murayama, M., Yasutake, K., Takahashi, H., Yokoyama, M., and Ishiguro, K. (2001) Involvement of cyclin dependent kinase5 activator p25 on tau phosphorylation in mouse brain. *Neurosci. Lett.* **306**, 37–40
47. Bian, F., Nath, R., Sobocinski, G., Booher, R. N., Lipinski, W. J., Callahan, M. J., Pack, A., Wang, K. K., and Walker, L. C. (2002) Axonopathy, tau abnormalities, and dyskinesia, but no neurofibrillary tangles in p25-transgenic mice. *J. Comp. Neurol.* **446**, 257–266
48. Muyllaert, D., Terwel, D., Kremer, A., Sennvik, K., Borghgraef, P., Devijver, H., Dewachter, I., and Van Leuven, F. (2008) Neurodegeneration and neuroinflammation in cdk5/p25-inducible mice: a model for hippocampal sclerosis and neocortical degeneration. *Am. J. Pathol.* **172**, 470–485
49. Sadleir, K. R., Eimer, W. A., Cole, S. L., and Vassar, R. (2015) Aβ reduction in BACE1 heterozygous null 5XFAD mice is associated with transgenic APP level. *Mol. Neurodegener.* **10**, 1

Received for publication January 26, 2017.
Accepted for publication April 5, 2017.

Adeno-associated viral 9–mediated Cdk5 inhibitory peptide reverses pathologic changes and behavioral deficits in the Alzheimer's disease mouse model

Yong He, Suyue Pan, Miaojing Xu, et al.

FASEB J published online April 18, 2017
Access the most recent version at doi:10.1096/fj.201700064R